This is a self-archived – parallel published version of this article in the publication archive of the University of Vaasa. It might differ from the original.

Minimizing wind power curtailment using a continuous-time risk-based model of generating units and bulk energy storage

Author(s): Nikoobakht, Ahmad; Aghaei, Jamshid; Shafie-khah, Miadreza; Catalão, J.P.S.

Title: Minimizing wind power curtailment using a continuous-time risk-based model of generating units and bulk energy storage

Year: 2020

Version: Final draft (post print, aam, accepted manuscript)

Please cite the original version:

Nikoobakht, A., Aghaei, J., Shafie-khah, M., & Catalão, J. P. S., (2020). Minimizing wind power curtailment using a continuous-time risk-based model of generating units and bulk energy storage. IEEE Transactions on Smart Grid. https://doi.org/10.1109/TSG.2020.3004488.

Minimizing Wind Power Curtailment using a Continuous-Time Risk-Based Model of Generating Units and Bulk Energy Storage

Ahmad Nikoobakht, *Member, IEEE,* Jamshid Aghaei, *Senior Member, IEEE,* Miadreza Shafie-khah, *Senior Member, IEEE,* and J.P.S. Catalão, *Senior Member, IEEE*

Abstract—Wind power curtailment (WPC) occurs because of the non-correlation between wind power generation (WPG) and load, and also due to the fast sub-hourly variations of WPG. Recently, advances in energy storage technologies facilitate the use of bulk energy storage units (ESUs) to provide the ramping required to respond to fast sub-hourly variations of WPGs. To minimize the sub-hourly WPC probability, this paper addresses a generic continuous-time risk-based model for sub-hourly scheduling of energy generating units and bulk ESUs in the day-ahead unit commitment (UC) problem. Accordingly, the Bernstein polynomials are hosted to model the continuous-time risk-based UC problem with ESU constraints. Also, the proposed continuous-time risk-based model ensures that the generating units and ESUs track the sub-hourly variations of WPG, while the load and generation are balanced in each sub-hourly intervals. Finally, the performance of the proposed model is demonstrated by simulating the IEEE 24-bus Reliability and Modified IEEE 118-bus test systems.

Index Terms—Wind power curtailment, continuous-time unit commitment, Bernstein polynomials and energy storage.

NOTATION

A. Indices

j	Index of Bernstein basis function.
w, g, e	Index for generation units, wind farms and ESUs, respectively.
s	Index of scenarios.
t	Index of continuous-time.
t'	Index of discrete-time.
$(\bullet)^s$	Related to scenario s.
$(\bullet)_{(\cdot),t}$	Related to element $(\cdot)$ at time period t.

B. Parameters

c_g	Cost of a generating unit.
c_w	Curtailment cost of the wind turbine w.
c_g^{su}	Startup cost of a generating unit .

$\overline{G}_g / \underline{G}_g$	Max/min output of a generating unit.
$\ddot{G}_g / \dot{G}_g$	Max/min ramp rate for a generating unit.
π_s	Probability of scenario s.
DT_g / UT_g	Minimum off/on time of a generating unit.
$W_{f,wt} / D_{nt}$	Wind power/load forecasted.
b_{nm}	Susceptance of a transmission line.
$\overline{f}_k$	Max power flow on a transmission line.
η_e^c / η_e^d	Charge/discharge efficiency of a ESU.
$\overline{g}_e / \overline{d}_e$	Max discharge/charge power of a ESU.
$\underline{E}_e / \overline{E}_e$	Min/max energy capacity for a ESU.
$\dot{d}_e / \ddot{d}_e$	Min/max ramp rate of ESU's charging power.
$\dot{g}_e / \ddot{g}_e$	Min/max ramp rate of ESU's dischargin.
$\underline{R}_g / \overline{R}_g$	Maximum ramp up/down rate for a generating unit.
$b_{j,J}^t$	Bernstein basis function of order J.
$\Im_J^{f_t}$	Bernstein polynomial operator over function $f(t)$.
$C_{j,J}^{(\bullet)}$	Bernstein coefficient of $(\bullet)$.
J	Order of Bernstein polynomial.
M	Large enough constant.
β	Risk aversion parameter.
λ	Probability of wind power curtailment.

C. Variables

G_{gt}	Power generation of a generating unit.
$\overline{\Delta G}_{gt}^s / \underline{\Delta G}_{gt}^s$	Upward/downward capacity of reserve.
ΔW_{wt}^s	Wind power curtailment.
$z_{g,t} / y_{gt}$	Shutdown/startup binary variable for a generating unit.
I_{gt}	Binary variable for state of a generating unit .
Ψ^s	Binary variable related to scenario s.
$\dot{G}_{gt}$	Ramp up rate for a generating unit.
g_{et} / d_{et}	Discharge/charge power of ESU.
f_{kt}	Power flow on a transmission line.
θ_{nt}	Voltage angle at bus at a bus.
$\underline{E}_e / \overline{E}_e$	Min/max energy capacity for a ESU.
E_{et}	State of charge for a ESU.
$\dot{d}_{et} / \dot{g}_{et}$	Ramp up rate for discharge/charge power of a ESU.
$\vec{C}_J^{(\bullet)}$	Vector containing Bernstein coefficients of $(\bullet)$.
$\tilde{C}$	Expected operation cost.

I. INTRODUCTION

A. Background and Motivation

IN recent years, utilization of wind power generation (WPG) is expected to increase fast sub-hourly variations and generation uncertainty in the power system operation. In this condition the power system operators are faced with two key challenges: i) fast sub-hourly variations of WPG and ii) wind generation uncertainty. In other to management two mentioned challenges, two main options are available for a power system operator. The first option is wind power curtailment (WPC), however, this option is unattractive. In fact, the insufficient fast up/down ramping capability and reserve capacity in power system operation are the common reasons for involuntary WPC [1] and [2]. Accordingly, to provide fast up/down ramping capability, two general options have been suggested: (i) commitment of fast-ramp gas-fired generation units (GFUs), (ii) using bulk energy storage units (ESUs), i.e., battery energy storage system or pump storage systems with high ramping capability [3], [4]. However, utilization of the GFUs are faced two main challenges: i) whether the GFUs can be dispatched in real-time since it needs a "just-in-time" supply of the natural gas delivery system, ii) in cold seasons, generation costs for the GFUs are high, because natural gas productions are scheduled to supply residential and commercial customers for heating purposes. Accordingly, natural gas supply availability would directly impact on mitigating uncertainty and variability of WPG and operation costs. Under those circumstances, the second option, i.e., the bulk ESUs, with fast-response capabilities, i.e., fast power dispatch and fast ramping capabilities, can play a vital role to compensate fast sub-hourly variations and uncertainty of WPG. Ref [5] presented a method to operation of bulk ESUs capacity to maximize WPG utilization in a unit commitment problem. Ref [1], the ESUs have been utilized as appropriate tools with the fast ramping capability to cope with the WPG uncertainty by storing the excess wind energy once the generation is higher than the forecasted values, then, using stored wind energy to avoid the penalties associated with generating less wind power than the forecasted values. Ref [6], fast ramping capability of utility-scale ESUs is leveraged to maintain the short-term loading of transmission lines within limits in case of N - 1 transmission line contingencies. Ref [7] discuss thoroughly the large-scale ESU utilization challenges in a power system with high renewable recourse integration. In [8] used utility-scale energy storage sources as part of the set of control measures in a corrective form of the security-constrained unit commitment problem. Ref [9], presented and analyzed two models for the hourly scheduling of centralized and distributed electric energy storage in day-ahead electricity markets. In [10] hourly optimal grid reconfiguration and electric vehicle mobility fleets (as distribute energy storages) have been used as the remedial action to enhance the system flexibility to handle wind uncertainties. In Refs [1]- [10], the effect of utility-scale ESUs on power system operation studied but they only focused on traditional discrete-time operation methods. In fact, the traditional discrete-time (CT) operation method has worked well for compensating the variability of loads in the past, but it is starting to fall short, as increasing WPGs add sub-hourly variability to the power system and large sub-hourly ramping events happen much more commonly. Similarly, it is impossible to instantaneously ramp up/down at the hourly intervals, thus, with the UC model cannot manage fast ramping capability of ESUs and compensate sub-hourly variations of WPG

in power system operation. Accordingly, the scarcity of ramping resources is occurred. In fact, the scarcity of ramping resources is a phenomenon that occurs once the electrical power system has enough ramping capacity but it is unable to acquire ramping requirements to respond to sub-hourly WPG variations. In order to address this challenge, in this paper a continuous-time (CT) model based on Bernstein polynomial functions is adopted which allows to better capture the ramping capabilities of the ESUs because it provides a more accurate representation of the sub-hourly ramping needs to follow fast sub-hourly variations of WPG. The CT model is appropriate for managing fast sub-hourly variations of WPG, but the risk assessment of sub-hourly WPC in power system operation cannot be addressed by this model. Recently, the application of risk-based assessment techniques for power system operation with WPG has attracted high interest from electrical power industry [11], [12] and [13]. The literature on the continuous-time operation model can be reached in [14], [15] and [16]. However, the model proposed in this paper differs from the above references in five aspects:
- The continuous-time model for ESU has been not presented.
- The network security constraints have not been considered by continuous-time. - No literature has investigated the effect of fast-ramping resources in continuous-time framework on handling real-time WPG uncertainty. - The uncertainty of wind has not been investigated in [15] and [16]. Also, the proposed operation model in [15] and [16] is deterministic not stochastic. For example, in [12] and [13] a two-stage stochastic risk assessment method are also used to operation problems under significant WPG. Also, in [12] the authors propose a risk assessment approach to the quantitative evaluation of security of power systems with significant WPG for short-term operation planning. Similarly, in [17] the authors use Value at risk (VaR) and integrated risk management indexes separately to assess the risk, so that an optimal tradeoff between the profit and risk is made for the system operations. In [18] develops risk-constrained bidding strategy in unit commitment that generation company (GENCO) participates in energy and ancillary services markets. In this paper risk-constrained has been modeled in a three-stage stochastic operation problem. In [19] proposed a multi-stage stochastic risk model to make optimal investment decisions on wind power facilities along a multi-stage horizon. The main weakness in these studies include: i) In these references, the risk of WPC has been overlooked in power system operation. ii) With proposed risk models in [11], [12] and [13] cannot address risk assessment of sub-hourly WPC in an operation problem. In fact, the risk models in these references are based on traditional CT method. Accordingly, in this paper has been proposed a novel continuous-time risk assessment approach, which can assess risk of the sub-hourly WPC. In summary, the proposed risk model can minimize the sub-hourly WPC probability of a wind farm under fast sub-hourly variations in power system. In other word, the proposed continuous-time risk model is a conceptual complement providing a better measure of the continuous-time WPC probability. The higher the risk the higher sub-hourly WPC in undesired scenarios, and vice versa. Though continuous-time risk of WPC in all undesired scenarios and all sub-hourlies cannot be eliminated fully due to probabilistic behaviors of continuous-time WPG variations, it can be assessed and managed within an acceptable level in power system operation.

B. The Main Contribution

The aim of this paper is developing a fundamental, analytically tractable and general model for joint scheduling of GUs and ESUs in a risk-based operation problem. The risk-based operation problem is formulated as a continuous-time framework, which schedules for optimal continuous-time power and ramping routes of generator units and ESUs to compensate fast sub-hourly variation of WPG trajectory over the operating horizon.

Furthermore, a function space-based method is implemented to solve the proposed continuous-time problem. In fact, continuous-time problem is a non-convex mixed integer non-linear programming (MINLP) model. Accordingly, the MINLP model is intractable to be solved by traditional MINLP solvers [20]. Consequently, the proposed continuous-time risk model may not be a tractable problem even for small size systems which boost research on to develop an efficient tractable solution method for it. In the proposed solution method, the continuous-time generation and ramping routes of GUs as well as the energy, power and ramping routes of ESUs are modeled by Bernstein polynomials. The proposed technique converts the continuous-time risk model into a mixed integer linear programming (MILP) problem with the Bernstein coordinates of decision routes as decision variables. Noted that, the Bernstein polynomials have convex hull property, thus, here this property is utilized to efficiently impose the continuous-time inequality constraints, including the power, energy and ramping constraints of ESUs. The main advantage of the proposed solution method allows for full exploitation of the ESU capabilities through higher-order solution spaces, while including, as a special case, the traditional DT solution through the zeroth order Bernstein polynomial approximation. The other major contributions of this paper are outlined below:

(i) This study describes the continuous-time ramping model of ESUs as time derivatives of their power trajectories, capturing their sub-hourly ramping capability to cover the fast ramping necessity of fast sub-hourly variations of WPG.

(ii) This paper proposes a new continuous-time risk assessment model which can assesses probability of WPC in sub-hourly intervals. Nevertheless, the proposed risk model in this paper differs from the previous risk model in two aspects: i) with other risk assessment models cannot minimize probability of WPC sub-hourly intervals over the scheduling horizon, ii) with this proposed risk assessment model can better response to uncertainty of WPG in sub-hourly intervals. But these features are ignored in previous risk models, e.g., VaR.

II. CONTINUOUS-TIME DAY-AHEAD SCHEDULING MODEL

A. Modeling Assumptions

The assumptions considered in this paper are as follows:
(i) The linear cost function for generating units are considered [21].
(ii) In order for uncertainty modeling, several approaches and techniques have been introduced such as fuzzy programming and stochastic programming. Since stochastic programming approach has less complexity, this approach is applied in this paper. For the sake of simplicity, only WPG uncertainty is considered. Nevertheless, other uncertainties such as load uncertainty and

(lines') generators' availability can be incorporated into the proposed model. The uncertainty of WPG is modeled through a set of reasonable scenarios based on the available forecasted data. It should be noted that scenario generation and reduction techniques are beyond the scope of this paper.
(iii) A DC power flow model is used.

B. Formulation

The original continuous-time day-ahead scheduling problem is a kind of two-stage stochastic optimization to minimize the system operation cost during the scheduling period subject to the first-stage and second-stage constraints.

$$
\begin{aligned}
\min \ & \sum_g \left(\int_T \left(c_g G_{gt} + c_g^{SU} y_{gt} \right) dt \right) \\
& + \sum_s \left(\pi_s \int_T c_g \left(\bar{\Delta} G_{gt}^s + \underline{\Delta} G_{gt}^s \right) dt + \sum_w \pi_s \int_T c_w \Delta W_{wt}^s dt \right)
\end{aligned}
\tag{1}
$$

The first term of (1), i.e., here-and-now, refers to the generation cost plus start up cost of generating units at the base case, while, the second term, i.e., wait-and-see, represents the cost of up and down reserve deployments, respectively. It should be noted that, the up and down reserve deployments cost refers to the generation cost of the additional power generated in the real-time operation to offset the power imbalance occurred due to WPG variability. The last term of (1) is the WPC cost.

-The first-stage constraints are:

$$
\underline{G}_g I_{gt} \leq G_{gt} \leq \overline{G}_g I_{gt} \tag{2}
$$

$$
\int_t^{t-UT_g+1} I_{g,t'} dt' \leq UT_g y_{g,t} \tag{3}
$$

$$
\int_t^{t-DT_g+1} \left(1 - I_{g,t'} \right) dt' \leq DT_g z_{g,t} \tag{4}
$$

$$
y_{g,t} - z_{g,t} = I_{g,t} - I_{g,t-1} \tag{5}
$$

$$
\underline{\dot{G}}_g I_{gt} \leq \frac{dG_{gt}}{dt} = \dot{G}_{gt} \leq \overline{\dot{G}}_g I_{gt} \tag{6}
$$

$$
\begin{aligned}
& \sum_{g(n)} G_{gt} + \sum_{w(n)} W_{f,wt} + \sum_{e(n)} g_{et} \\
& - \sum_{k(n,m)} f_{kt} + \sum_{k(m,n)} f_{kt} = D_{nt} + \sum_{e(n)} d_{et}
\end{aligned}
\tag{7}
$$

$$
-\overline{f}_k \leq f_{kt} = b_{nm} \cdot (\theta_{nt} - \theta_{mt}) \leq \overline{f}_k \tag{8}
$$

$$
\frac{dE_{et}}{dt} = \eta^c d_{et} - \frac{g_{et}}{\eta^d} \tag{9}
$$

$$
0 \leq d_{et} \leq \overline{d}_e \tag{10}
$$

$$
0 \leq g_{et} \leq \overline{g}_e \tag{11}
$$

$$
\underline{E}_e \leq E_{et} \leq \overline{E}_e \tag{12}
$$

$$
\underline{\dot{d}}_e \leq \frac{d(d_{et})}{dt} = \dot{d}_{et} \leq \overline{\dot{d}}_e \tag{13}
$$

$$\underline{\dot{g}}_e \leq \frac{d(g_{et})}{dt} = \dot{g}_{et} \leq \overline{\dot{g}}_e \tag{14}$$

$$G_{g,t=0} = G_g^0, g_{e,t=0} = g_e^0, d_{e,t=0} = d_e^0, E_{e,t=0} = E_e^0 \tag{15}$$

Constraint (2) impose the lower and upper limits for power route of GUs, respectively. Equations (3) and (4) enforce the minimum on and off time constraints. Constraint (5) is required to guarantee that $y_{g,t}$ and $z_{g,t}$ take the suitable values once a GU is either turned on or off. Continuous-time up and down ramping route constraint is shown in (6). Noted that, the associated ramping routes of GUs are determined by means of derivation of the power generation routes with respect to time. The spontaneous power balance constraint for each bus is forced by (7). Constraint (8) imposes that the line flows stay within their capacity limits. The state of charge of ESUs is controlled using the continuous-time differential equation (9) during the scheduling period. In this equation, η^c/η^d refers to the charging/discharging efficiency, respectively. The limitations on the continuous-time power charging/ discharging, stored energy and charging/ discharging ramping routes over T for each ESU, are imposed by (10) – (14), respectively, wherein the min and max limits of the routes have been denoted by the underlined and overlined constant terms, respectively. Noted that, the associated ramping routes of charging/discharging of ESUs are determined by means of derivation of the charging/discharging routes with respect to the time. The starting (initial) values for the state routes are stated in (15) wherein G_g^0, g_e^0, d_e^0, and E_e^0 are constant initial values of each decision variable. *-The second-stage constraints are:*

$$\sum_{g(n)} \left(G_{gt} + \bar{\Delta} G_{gt}^s - \underline{\Delta} G_{gt}^s \right) + \sum_{w(n)} \left(W_{f,wt}^s - \Delta W_{wt}^s \right)$$
$$+ \sum_{e(n)} g_{et}^s - \sum_{k(n,m)} f_{kt}^s + \sum_{k(m,n)} f_{kt}^s = D_{nt} + \sum_{e(n)} d_{et}^s \tag{16}$$

$$\underline{G}_g I_{gt} \leq \left(G_{gt} + \overline{\Delta} G_{gt}^s - \underline{\Delta} G_{gt}^s \right) \leq \overline{G}_g I_{gt} \tag{17}$$

$$0 \leq \Delta W_{wt}^s \leq W_{f,wt}^s \tag{18}$$

$$0 \leq \overline{\Delta} G_{gt}^s / \underline{\Delta} G_{gt}^s \leq \overline{R}_g I_{gt} / \underline{R}_g I_{gt} \tag{19}$$

$$(8) - (15) \tag{20}$$

Constraint (16) denotes the continuous-time power balance at the real-time operation for each scenario. The limits of GUs' power generation, WPC and up/down reserves are provided in (17) – (19), respectively, for each scenario. Here, $\overline{\Delta} G_{gt}^s$ and $\underline{\Delta} G_{gt}^s$ represents the physically acceptable adjustments of GUs' power generation in ten continuous-time minutes to absorb the wind power variability. The constraint (20) enforces constraints (8) – (15). It is noted that in these constraints the variables $\left\{ f_{kt}, \ \theta_{nt}, E_{et}, d_{et}, g_{et}, \dot{d}_{et}, \dot{g}_{et} \right\}$ are replaced by $\left\{ f_{kt}^s, \ \theta_{nt}^s, E_{et}^s, d_{et}^s, g_{et}^s, \dot{d}_{et}^s, \dot{g}_{et}^s \right\}$, respectively.

III. REFORMULATION OF CONTINUOUS-TIME DAY-AHEAD SCHEDULING PROBLEM USING BERNSTEIN POLYNOMIALS

The proposed stochastic risk problem based on the continuous-time model, (1) – (20), has an uncompromising computational burden due to its unbounded solution space. That is, it is vital to reduce the dimensions of the continuous-time modeling to make it

tractable from the computational aspect. Accordingly, the proposed continuous-time modeling is reformulated based on a governable function space defined by Bernstein polynomials (BPs) while they are computationally tractable [22]. Here, the vector of polynomials of degree J as $b_{j,J}^t$ can be defined as follows:

$$b_{j,J}^t = \binom{J}{j} t^j (1-t)^{J-j} \tag{21}$$

For a function $f(t)$, defined on the interval $t \in [0,1]$, the expression $\Im_J^{f(t)}$ is called the BPs of order J for the function $f(t)$ as follows:

$$\Im_J^{f(t)} = \sum_{j=0}^J f\left(\frac{j}{J}\right) \cdot b_{j,J}^t \tag{22}$$

The coefficients $f\left(\frac{j}{J}\right)$ are called control points. If $f(t)$ is continuous on $t \in [0,1]$, it is proven that the following equation is true for $t \in [0,1]$.

$$\lim_{J \to \infty} \Im_J^{f(t)} = f(t) \tag{23}$$

Another property of the BPs is that the coefficients of a polynomial's derivative with degree $J-1$ are the finite differences of the original coefficients with degree J:

$$\dot{\Im}_{J-1}^{f_t} = J \sum_{j=0}^{J-1} \left\{ f\left(\frac{j+1}{J}\right) - f\left(\frac{j}{J}\right) \right\} \binom{J-1}{j} t^j (1-t)^{J-j-1} \tag{24}$$

Hence, the elements of $\dot{b}_{j,J}^t$, can be introduced to translate the derivatives of $b_{j,J}^t$ into the same family of polynomials of degree $J-1$. Each BP of order J, is consisted of J different terms, each of them is the production of a coefficient, $f\left(\frac{j}{J}\right)$, and a Bernstein basis function, $b_{j,J}^t$. Convex hull property indicates that $\Im_J^{f(t)}$ is always strictly placed inside of the convex hull formed by Bernstein coefficients for each j as the control polygon. That is, $\Im_J^{f(t)}$ is always between max and min coefficients as follows:

$$\min_{\forall j} \left\{ f\left(\frac{j}{J}\right) \right\} \leq \Im_J^{f(t)} \leq \max_{\forall j} \left\{ f\left(\frac{j}{J}\right) \right\} \tag{25}$$

$$\min_{\forall j} \left\{ f\left(\frac{j+1}{J}\right) - f\left(\frac{j}{J}\right) \right\} \leq \dot{\Im}_{J-1}^{f_t} \leq \max_{\forall j} \left\{ f\left(\frac{j+1}{J}\right) - f\left(\frac{j}{J}\right) \right\} \tag{26}$$

These properties significantly help us later, when max and min generations and ramping constraints are driven. In the following, the continuous-time approximation of the wind power and load profiles and equations (1) – (20) are modeled based on the proposed BPs.

A. Load and Wind Profiles

Load profile approximation: the continuous-time approximation of the load can be reformulated for sub-interval j of each hour using the BPs of degree J, i.e., $\{b_{0,J}^t, b_{1,J}^t, ..., b_{J,J}^t\}$ while the load quantity at the jth sub-intervals of the hour t' is considered as the weighting factors, as follows:

$$\begin{cases} \Im_J^{D_{n,t}} = \sum_{j=0}^J \overbrace{D_{n,\left(t'+\frac{j}{J}\right)}}^{C_j^{D_{n,t'}}} \cdot \binom{J}{j} \cdot (t-t')^j \cdot (1-(t-t'))^{J-j} \\ \forall t \in [t', t'+1] \end{cases} \tag{27}$$

To show this equation in matrix form, it can be divided into the product of Bernstein coefficients and Bernstein basis functions as follows:

$$\Im_J^{D_n,t} = \begin{bmatrix} C_{0,J}^{D_n,t'} & C_{1,J}^{D_n,t'} & \cdots & C_{J,J}^{D_n,t'} \end{bmatrix} \begin{bmatrix} b_{0,J}^{t-t'} \\ b_{1,J}^{t-t'} \\ \vdots \\ b_{J,J}^{t-t'} \end{bmatrix} = \vec{C}_J^{D_n,t'} \vec{b}_J^{t-t'}$$

(28)

According to (23), with a large enough J, the deviation of the main function and its Bernstein approximation will be small. - Wind profile approximation: It is also required to assign a BP based representation to have a continuous-time approximation of wind power profile analogous to the load profile.

$$\Im_J^{W_w,t} = \vec{C}_J^{W_w,t'} \vec{b}_J^{t-t'}, \forall t \in [t', t'+1] \quad (29)$$

Noted that, the vector $\vec{C}_J^{W_w,t'}$ and $\vec{C}_J^{D_n,t'}$ are similar.

B. The GU Constraints

The generation routes of GUs, $G_{g,t}$, in the Bernstein function space are defined by (30):

$$\underline{G}_g I_{g,t'} \leq \Im_J^{G_g,t} = \vec{C}_J^{G_g,t'} \vec{b}_J^{t-t'} \leq \overline{G}_g I_{g,t'}, \forall t \in [t', t'+1] \quad (30)$$

where $\vec{C}_J^{G_g,t'} = \begin{bmatrix} C_{0,J}^{G_g,t'}, C_{1,J}^{G_g,t'}, ..., C_{J,J}^{G_g,t'} \end{bmatrix}$ is J-dimensional vector of Bernstein coefficients of GU generation routes.

According to (25), $\Im_J^{G_g,t}$ is always between max and min generation limits.

$$\underline{G}_g I_{g,t'} \leq \vec{C}_J^{G_g,t'} \leq \overline{G}_g I_{g,t'} \quad (31)$$

C. The GU Ramping Route:

According to (26), the continuous-time ramping route of GU with limitations is modeled by the BPs of degree $J-1$ as:

$$\underline{\dot{G}}_g I_{g,t'} \leq \dot{\Im}_{J-1}^{G_g,t} = J\vec{C}_{J-1}^{G_g,t'} \vec{b}_{J-1}^{t-t'} \leq \overline{\dot{G}}_g I_{g,t'} \quad (32)$$

$$\vec{C}_{J-1}^{G_g,t'} = \begin{bmatrix} C_{1,J-1}^{G_g,t'} - C_{0,J-1}^{G_g,t'}, \cdots, C_{J-1,J-1}^{G_g,t'} - C_{J-2,J-1}^{G_g,t'} \end{bmatrix} \quad (33)$$

According to (26), to put a limitation on the continuous-time ramping route of Gus, the following equation should be satisfied:

$$\frac{\underline{\dot{G}}_g I_{g,t'}}{J} \leq \vec{C}_{J-1}^{\dot{G}_g,t'} \leq \frac{\overline{\dot{G}}_g I_{g,t'}}{J} \quad (34)$$

D. The Minimum Up/Down Time Constraints:

It is assumed that the commitment and therefore shut-down and start-up variables are constant within each interval and equal to the commitment, shut-down and start-up decisions at the beginning of the interval t.

$$\sum_{t'}^{t'-UT_g+1} I_{g,t'} \leq UT_g y_{g,t'} \quad (35)$$

$$\sum_{t'}^{t'-DT_g+1} (1 - I_{g,t}) \leq DT_g z_{g,t'} \quad (36)$$

E. The Charging/Discharging Constraints:

The charging and discharging power routes of ESU with its min and max routes limits can be modeled by (37) – (38):

$$0 \leq \Im_J^{d_e,t} = \vec{C}_J^{d_e,t'} \vec{b}_J^{t-t'} \leq \overline{d}_e \Rightarrow 0 \leq \vec{C}_J^{d_e,t'} \leq \overline{d}_e \quad (37)$$

$$0 \leq \Im_J^{g_e,t} = \vec{C}_J^{g_e,t'} \vec{b}_J^{t-t'} \leq \overline{g}_e \Rightarrow 0 \leq \vec{C}_J^{g_e,t'} \leq \overline{g}_e \quad (38)$$

where $\vec{C}_J^{d_e,t'} = \begin{bmatrix} C_{0,J}^{d_e,t'}, C_{1,J}^{d_e,t'}, ..., C_{J,J}^{d_e,t'} \end{bmatrix}$ and $\vec{C}_J^{g_e,t'} = \begin{bmatrix} C_{0,J}^{g_e,t'}, C_{1,J}^{g_e,t'}, ..., C_{J,J}^{g_e,t'} \end{bmatrix}$ are J-dimensional vectors of the Bernstein coefficients of charging and discharging power routes, respectively.

F. The Charging/Discharging Ramping Route:

Here similar to GU ramping route, the continuous-time ramping route of ESUs with limitations are modeling by the BPs of degree $J-1$ as:

$$\underline{\dot{d}}_e \leq \dot{\Im}_{J-1}^{\dot{d}_e,t} = J\vec{C}_{J-1}^{d_e,t'} \vec{b}_{J-1}^{t-t'} \leq \overline{\dot{d}}_e \Rightarrow \frac{\underline{\dot{d}}_e}{J} \leq \vec{C}_{J-1}^{d_e,t'} \leq \frac{\overline{\dot{d}}_e}{J} \quad (39)$$

$$\underline{\dot{g}}_e \leq \dot{\Im}_{J-1}^{\dot{g}_e,t} = J\vec{C}_{J-1}^{g_e,t'} \vec{b}_{J-1}^{t-t'} \leq \overline{\dot{g}}_e \Rightarrow \frac{\underline{\dot{g}}_e}{J} \leq \vec{C}_{J-1}^{d_e,t'} \leq \frac{\overline{\dot{g}}_e}{J} \quad (40)$$

where $\vec{b}_{J-1}^{t-t'}$ is the J-dimensional vectors relating $b_{j,J-1}^{t-t'}$ and also $\vec{C}_{J-1}^{d_e,t'} = \begin{bmatrix} C_{1,J-1}^{d_e,t'} - C_{0,J-1}^{d_e,t'}, ..., C_{J-1,J-1}^{d_e,t'} - C_{J-2,J-1}^{d_e,t'} \end{bmatrix}$ and $\vec{C}_{J-1}^{g_e,t'} = \begin{bmatrix} C_{1,J-1}^{g_e,t'} - C_{0,J-1}^{g_e,t'}, ..., C_{J-1,J-1}^{g_e,t'} - C_{J-2,J-1}^{g_e,t'} \end{bmatrix}$ are the J-dimensional vectors of Bernstein coefficients associated with ESU charge and discharge ramping routes.

G. The Energy Route of ESU:

By integrating the state equation (9) over t, the routes of energy storage of ESU are driven by the BPs of degree $J+1$. Noted that, the integral of BPs of degree J are linearly associated with BPs of degree $J+1$.

$$\begin{cases} \int_0^t \frac{dE_{et}}{dt} = \int_0^t \left(\eta^c d_{et} - \frac{g_{et}}{\eta^d} \right) = \int_0^t \frac{d\Im_J^{E_e,t}}{dt} \\ \quad = \int_0^t \left(\eta^c \Im_J^{d_e,t} - \frac{\Im_J^{g_e,t}}{\eta^d} \right) \\ \Im_J^{E_e,t} = \vec{C}_J^{E_e,t'} \vec{b}_J^{t-t'} \end{cases} \quad (41)$$

$$\Im_{J+1}^{E_e,t} - \Im_{J+1}^{E_e,0} = \left(\eta^c \Im_{J+1}^{d_e,t} - \frac{\Im_{J+1}^{g_e,t}}{\eta^d} \right) \Rightarrow \vec{C}_{J+1}^{E_e,t'} \vec{b}_{J+1}^{t-t'} - \vec{C}_{J+1}^{E_e,0} \vec{b}_{J+1}^{t-t'} =$$
$$\left(\eta^c \left(\vec{C}_{J+1}^{d_e,t'} \vec{b}_{J+1}^{t-t'} \right) - \left(\eta^d \right)^{-1} \left(\vec{C}_{J+1}^{g_e,t'} \vec{b}_{J+1}^{t-t'} \right) \right) \quad (42)$$

where $\vec{C}_{J+1}^{E_e,0}$ in (42) is the constant initial energy values vector E_e^0 that is modeled by $\vec{b}_{J+1}^{t-t'}$, and $\vec{C}_{J+1}^{E_e,t'}$ is a (J+1)-dimensional vector of Bernstein coefficients of ESU energy routes, equal to:

$$\vec{C}_{J+1}^{E_e,t'} - \vec{C}_{J+1}^{E_e,0} = \left(\eta^c \left(\vec{C}_{J+1}^{d_e,t'} \right) - \left(\eta^d \right)^{-1} \left(\vec{C}_{J+1}^{g_e,t'} \right) \right) \quad (43)$$

H. The line flow Constraints:

By substituting the line flow and voltage angle routes Bernstein models in line flow constraint (8), we have:

$$\begin{cases} \Im_J^{f_{k,t}} = b_{nm} \cdot \left(\Im_J^{\theta_{n,t}} - \Im_J^{\theta_{m,t}} \right) \Rightarrow \vec{C}_J^{f_{k,t'}} = b_{nm} \cdot \left(\vec{C}_J^{\theta_{n,t'}} - \vec{C}_J^{\theta_{m,t'}} \right) \\ \Im_J^{\theta_{n,t}} = \vec{C}_J^{\theta_{n,t'}} \vec{b}_J^{t-t'} \end{cases}$$
$$(44)$$

Then, the continuous-time limits on the line flow and voltage angle routes are enforced by controlling the Bernstein coefficients inside their limits, (21)–(22), for each sub-interval.

$$\underline{\theta}_n \le \vec{C}_J^{\theta_{n,t'}} \le \overline{\theta}_n \tag{45}$$

$$-\overline{f}_k \le \vec{C}_J^{f_{k,t'}} \le \overline{f}_k \tag{46}$$

I. Power Balance Constraint:

With replacing the BP models represented by (27), (28), (30), (36) and (37) in the power balance constraint (7), the following BP based power balance equation is driven:

$$\sum_{g(n)} \vec{C}_J^{G_{g,t'}} \vec{b}_J^{t-t'} + \sum_{w(n)} \vec{C}_J^{W_{w,t'}} \vec{b}_J^{t-t'} + \sum_{e(n)} \vec{C}_J^{g_{e,t'}} \vec{b}_J^{t-t'}$$
$$- \sum_{k(n,m)} \vec{C}_J^{f_{k,t'}} \vec{b}_J^{t-t'} + \sum_{k(m,n)} \vec{C}_J^{f_{k,t'}} \vec{b}_J^{t-t'}$$
$$= \vec{C}_J^{D_{n,t'}} \vec{b}_J^{t-t'} + \sum_{e(n)} \vec{C}_J^{d_{e,t'}} \vec{b}_J^{t-t'}$$
$$(47)$$

By removing $\vec{b}_J^{t-t'}$ from both sides, we have:

$$\sum_{g(n)} \vec{C}_J^{G_{g,t'}} + \sum_{w(n)} \vec{C}_J^{W_{w,t'}} + \sum_{e(n)} \vec{C}_J^{g_{e,t'}}$$
$$- \sum_{k(n,m)} \vec{C}_J^{f_{k,t'}} + \sum_{k(m,n)} \vec{C}_J^{f_{k,t'}} = \vec{C}_J^{D_{n,t'}} - \sum_{e(n)} \vec{C}_J^{d_{e,t'}}$$
$$(48)$$

Also, like constraint (7), the second stage continuous-time power balance constraint (16) can be adopted by Bernstein models as follows:

$$\sum_{g(n)} \left(\vec{C}_J^{G_{g,t'}} + \vec{C}_J^{\bar{\Delta} G_{g,t'}^s} - \vec{C}_J^{\Delta G_{g,t'}^s} \right) + \sum_{w(n)} \left(\vec{C}_J^{W_{w,t'}^s} - \vec{C}_J^{\Delta W_{w,t'}^s} \right)$$
$$+ \sum_{e(n)} \vec{C}_J^{g_{e,t'}^s} - \sum_{k(n,m)} \vec{C}_J^{f_{k,t'}^s} + \sum_{k(m,n)} \vec{C}_J^{f_{k,t'}^s} = \vec{C}_J^{D_{n,t'}^s} - \sum_{e(n)} \vec{C}_J^{d_{e,t'}^s}$$
$$(49)$$

Noted that, like vectors of Bernstein coefficients, i.e., $\vec{C}_J^{G_{g,t'}}$, the $\vec{C}_J^{\bar{\Delta} G_{g,t'}^s}, \vec{C}_J^{\Delta G_{g,t'}^s}$ and $\vec{C}_J^{\Delta W_{w,t'}^s}$ can be calculated analogously. Constraints (48) and (49) convert the continuous-time power balance constraints (7) and (16) to an algebraic form of the traditional discrete-time power balance equation on the Bernstein coefficients.

J. Continuity of Power and Ramping Routes:

- *Continuity of Power Routes:* As described before, in each interval t', both generation (wind power, GU generation and ESU discharging) and demand (ESU charging) are presented by J-dimensional vectors of Bernstein coefficients. For continuity of generation of GU and ESU charging and discharging routes between intervals, the first Bernstein coefficient of t' interval, should always be equal to the last Bernstein coefficient of the previous interval $t' - 1$ as follows:

$$\left\{ C_{0,J}^{G_{g,t'}} = C_{J,J}^{G_{g,t'-1}}, C_{0,J}^{d_{e,t'}} = C_{J,J}^{d_{e,t'-1}}, C_{0,J}^{g_{e,t'}} = C_{J,J}^{g_{e,t'-1}} \right\} \tag{50}$$

But, there is a problem with the continuity of generation of GU that should be resolved. This continuity constraint cannot be satisfied in times of starting-up or shutting-down of the GUs. To solve this issue, here, the continuity constraint $C_{0,J}^{G_{g,t'}} = C_{J,J}^{G_{g,t'-1}}$ is converted to (51) and (52) as:

$$C_{0,J}^{G_{g,t'}} \le C_{J,J}^{G_{g,t'-1}} + M \cdot y_{g,t'} \tag{51}$$

$$C_{0,J}^{G_{g,t'}} \ge C_{J,J}^{G_{g,t'-1}} - M \cdot z_{g,t'} \tag{52}$$

Once the GU commitment binary variable remains unchanged, both $y_{g,t'}$ and $z_{g,t'}$ are zero and (51) and (52) become an equality constraint. Once a GU is starting up, (50) gives the permission and (51) allows GU to shut-down. M is a relatively large number, i.e., bigger than the capacity of the largest GU.

- *Continuity of Ramping Routes:* For GU, it is physically impossible to have instantaneous changes in ramping. Also, ESUs requires ramping continuity of the charging and discharging power routes. Accordingly, the differential of generation and charging/discharging power routes should also be continuous. According to (24), this constraint can be obtained for the same-length intervals as below:

$$\begin{cases} C_{1,J}^{G_{g,t'}} - C_{0,J}^{G_{g,t'}} = C_{J,J}^{G_{g,t'-1}} - C_{J-1,J}^{G_{g,t'-1}} \\ C_{1,J}^{d_{e,t'}} - C_{0,J}^{d_{e,t'}} = C_{J,J}^{d_{e,t'-1}} - C_{J-1,J}^{d_{e,t'-1}}, \\ C_{1,J}^{g_{e,t'}} - C_{0,J}^{g_{e,t'}} = C_{J,J}^{g_{e,t'-1}} - C_{J-1,J}^{g_{e,t'-1}} \end{cases} \tag{53}$$

Constraint (53) is a relation between the last two coefficients of t' interval and the first two coefficients of the previous interval and ensures that the ramping is continuous at the breakpoint of the adjacent intervals. But for GU, this constraint also should be relaxed when a GU is running to start up or shut down. Thus, the constraints (54) and (55) like (51) and (52) are employed to cope with this problem as below:

$$C_{1,J}^{G_{g,t'}} - C_{0,J}^{G_{g,t'}} \le C_{J,J}^{G_{g,t'-1}} - C_{J-1,J}^{G_{g,t'-1}} + M \cdot y_{g,t'} \tag{54}$$

$$C_{1,J}^{G_{g,t'}} - C_{0,J}^{G_{g,t'}} \ge C_{J,J}^{G_{g,t'-1}} - C_{J-1,J}^{G_{g,t'-1}} - M \cdot z_{g,t'} \tag{55}$$

K. Objective Function:

Firstly, it is noted that integrating over BPs is straightforward (assuming $t - t' \in [t', t' + 1]$) as follows:

$$\int_{t'}^{t'+1} C_{j,J}^{G_{g,t'}} b_{j,J}^{t-t'} dt = \frac{\sum\limits_{j=0}^{J} C_{j,J}^{G_{g,t'}}}{J+1} \tag{56}$$

According to (56), the objective function (1) can be converted to (57).

$$\min \tilde{C} = \sum_{t'} \sum_{g} \left(\frac{c_g \sum\limits_{j=0}^{J} C_{j,J}^{G_{g,t'}}}{J+1} + c_g^{SU} y_{gt'} \right) +$$
$$\sum_{t'} \sum_{s} \left(\frac{\pi_s}{J+1} \right) \left(c_g \sum_{j=0}^{J} \left(C_{j,J}^{\overline{\Delta} G_{g,t'}} + C_{j,J}^{\Delta G_{g,t'}} \right) + c_w \sum_{j=0}^{J} C_{j,J}^{\Delta W_{w,t'}} \right)$$
$$(57)$$

IV. MODELING CONTINUOUS-TIME RISK ASSESSMENT FOR WPC PROBABILITY

Risk assessment are needed for describing the risk associated with a given decision. In this condition, risk assessment enable us to compare two different decisions in terms of the risk involved. In the previous studies it is possible to find a wide set of risk assessment used for different applications. For example, in [23], the conditional value-at-risk model as one of the most applied risk indices has been used in the optimal remote controlled switch deployment problem. The risk model in [23] determines the number and location of remote controlled switches such that the expected profit is maximized while financial risk is minimized. In [24] a risk-based day-ahead scheduling problem based on information gap decision theory. The risk method is used to manage the profits risk of the electric vehicle aggregator caused by the information gap between the forecasted and actual electricity prices. In [25], proposed a risk aversion model to guarantees cost and benefit recovery for virtual power plants. Ref [26] a conditional value-at-risk (CVaR) measure is involved to quantitatively control the energy loss risk under emergency islanding. The literature on the risk models can be reached in [23]-[26]. However, the proposed risk model differs from the above references in -three aspects:

i) The risk models were used for the traditional discrete-time methods.

ii) Wind curtailment was not modelled by these references.

ii) Probability of energy loss cannot calculated by the risk models in [24].

iii) With proposed risk models in [23]- [25], the energy loss cannot be handled in each sub-hourly interval.

Accordingly, in this study, a new two-stage stochastic continuous-time risk-based problem has been proposed that minimizing the probability of the sub-hourly WPC in some unfavorable discrete set of scenarios. The proposed continuous-time risk model minimizing the operation cost and probability of sub-hourly WPC while meeting the first and second stages constraints. The outline of the model is described as follows:

Min: Objective function,

s.t.

1) Risk model constraints,
   -First stage security constraints:
2) Individual generator constraints (including min/max generation, min on/off time, startup/shutdown characteristics and ramp rate limits),

3) Power balance and power transmission line constraints,
4) Energy storage constraints,
5) Continuity constraints,
   -Second-stage security constraints:
6) Individual generator constraints (including min/max generation with up/down reserves),
7) Wind power curtailment,
8) Power balance and power transmission line constraints,
9) Up/down reserves limits,
10) Energy storage constraints,
11) Continuity constraints,

The detailed modeling is presented as follows:

$$\min \quad \left(10^{-\beta}\right)\tilde{C} + \beta\lambda \tag{58}$$

1) Risk model constraints

$$\vec{C}_{v,l}^{\Delta W_w^s(t)} \le M\Psi^s \tag{59}$$

$$\sum_s \pi_s \Psi^s \le \lambda \tag{60}$$

$$(57) \tag{61}$$

- The first-stage constraints are:

2) Individual generator constraints

$$\underline{G}_g I_{g,t'} \le \vec{C}_J^{G_{g,t'}} \le \overline{G}_g I_{g,t'} \tag{62}$$

$$\sum_{t'}^{t'-UT_g+1} I_{g,t'} \le UT_g y_{g,t'} \tag{63}$$

$$\sum_{t'}^{t'-DT_g+1} (1 - I_{g,t}) \le DT_g z_{g,t'} \tag{64}$$

$$y_{g,t} - z_{g,t} = I_{g,t} - I_{g,t-1} \tag{65}$$

$$\frac{\underline{\dot{G}}_g I_{g,t'}}{J} \le \vec{C}_{J-1}^{\dot{G}_{g,t'}} \le \frac{\overline{\dot{G}}_g I_{g,t'}}{J} \tag{66}$$

3) Power balance and power transmission line constraints,

$$\sum_{g(n)} \vec{C}_J^{G_{g,t'}} + \sum_{w(n)} \vec{C}_J^{W_{w,t'}} + \sum_{e(n)} \vec{C}_J^{g_{e,t'}}$$
$$- \sum_{k(n,m)} \vec{C}_J^{f_{k,t'}} + \sum_{k(m,n)} \vec{C}_J^{f_{k,t'}} = \vec{C}_J^{D_{n,t'}} - \sum_{e(n)} \vec{C}_J^{d_{e,t'}} \tag{67}$$

$$-\overline{f}_k \le \vec{C}_J^{f_{k,t'}} = b_{nm} \cdot \left(\vec{C}_J^{\theta_{n,t'}} - \vec{C}_J^{\theta_{m,t'}}\right) \le \overline{f}_k \tag{68}$$

4) Energy storage constraints,

$$\vec{C}_{J+1}^{E_{e,t'}} - \vec{C}_{J+1}^{E_{e,0}} = \left(\eta^c \left(\vec{C}_{J+1}^{d_{e,t'}}\right) - \left(\eta^d\right)^{-1}\left(\vec{C}_{J+1}^{g_{e,t'}}\right)\right) \tag{69}$$

$$0 \le \vec{C}_J^{d_{e,t'}} \le \overline{d}_e \tag{70}$$

$$0 \le \vec{C}_J^{g_{e,t'}} \le \overline{g}_e \tag{71}$$

$$\underline{E}_e \le \vec{C}_J^{E_{e,t'}} \le \overline{E}_e \tag{72}$$

$$\frac{\underline{\dot{d}}_e}{J} \le \vec{C}_{J-1}^{d_{e,t'}} \le \frac{\overline{\dot{d}}_e}{J} \tag{73}$$

$$\frac{\underline{\dot{g}}_e}{J} \le \vec{C}_{J-1}^{d_{e,t'}} \le \frac{\overline{\dot{g}}_e}{J} \tag{74}$$

5) Continuity constraints,

$$\left\{C_{0,J}^{G_{g,t'}} = C_{J,J}^{G_{g,t'-1}}, C_{0,J}^{d_{e,t'}} = C_{J,J}^{d_{e,t'-1}}, C_{0,J}^{g_{e,t'}} = C_{J,J}^{g_{e,t'-1}}\right\} \tag{75}$$

$$C_{0,J}^{G_{g,t'}} \le C_{J,J}^{G_{g,t'-1}} + M \cdot y_{g,t'} \tag{76}$$

$$C_{0,J}^{G_{g,t'}} \ge C_{J,J}^{G_{g,t'-1}} - M \cdot z_{g,t'} \tag{77}$$

$$C_{1,J}^{G_{g,t'}} - C_{0,J}^{G_{g,t'}} \le C_{J,J}^{G_{g,t'-1}} - C_{J-1,J}^{G_{g,t'-1}} + M \cdot y_{g,t'} \tag{78}$$

$$C_{1,J}^{G_{g,t'}} - C_{0,J}^{G_{g,t'}} \ge C_{J,J}^{G_{g,t'-1}} - C_{J-1,J}^{G_{g,t'-1}} - M \cdot z_{g,t'} \tag{79}$$

-The second-stage constraints are:

6) Individual generator constraints (including min/max generation with up/down reserves).

$$\underline{G}_g I_{gt} \le \left(\vec{C}_J^{G_{gt}} + \vec{C}_J^{\overline{\Delta}G_{gt}^s} - \vec{C}_J^{\underline{\Delta}G_{gt}^s}\right) \le \overline{G}_g I_{gt} \tag{80}$$

$$0 \leq \vec{C}_J^{\overline{\Delta} G_{gt}^s} / \vec{C}_J^{\underline{\Delta} G_{gt}^s} \leq \overline{R}_g I_{gt} / \underline{R}_g I_{gt} \qquad (81)$$

7) Wind power curtailment.

$$0 \leq \vec{C}_J^{\Delta W_{wt}^s} \leq \vec{C}^{W_{f,wt}^s} \qquad (82)$$

8) Power balance and power transmission line constraints,

$$\sum_{g(n)} \left(\vec{C}_J^{G_{g,t'}} + \vec{C}_J^{\overline{\Delta} G_{g,t'}^s} - \vec{C}_J^{\Delta G_{g,t'}^s} \right) + \sum_{w(n)} \left(\vec{C}_J^{W_{w,t'}^s} - \vec{C}_J^{\Delta W_{w,t'}^s} \right)$$
$$+ \sum_{e(n)} \vec{C}_J^{g_{e,t'}^s} - \sum_{k(n,m)} \vec{C}_J^{f_{k,t'}^s} + \sum_{k(m,n)} \vec{C}_J^{f_{k,t'}^s}$$
$$= \vec{C}_J^{D_{n,t'}^s} - \sum_{e(n)} \vec{C}_J^{d_{e,t'}^s}$$

$$(83)$$

$$-\overline{f}_k \leq \vec{C}_J^{f_{k,t'}^s} = b_{nm} \cdot \left(\vec{C}_J^{\theta_{n,t'}^s} - \vec{C}_J^{\theta_{m,t'}^s} \right) \leq \overline{f}_k \qquad (84)$$

10) Energy storage constraints,

$$\vec{C}_{J+1}^{E_{e,t'}^s} - \vec{C}_{J+1}^{E_{e,0}^s} = \left(\eta^c \left(\vec{C}_{J+1}^{d_{e,t'}^s} \right) - \left(\eta^d \right)^{-1} \left(\vec{C}_{J+1}^{g_{e,t'}^s} \right) \right) \qquad (85)$$

$$0 \leq \vec{C}_J^{d_{e,t'}^s} \leq \overline{d}_e \qquad (86)$$

$$0 \leq \vec{C}_J^{g_{e,t'}^s} \leq \overline{g}_e \qquad (87)$$

$$\underline{E}_e \leq \vec{C}_J^{E_{e,t'}^s} \leq \overline{E}_e \qquad (88)$$

$$\frac{\underline{\dot{d}}_e}{J} \leq \vec{C}_{J-1}^{d_{e,t'}^s} \leq \frac{\overline{\dot{d}}_e}{J} \qquad (89)$$

$$\frac{\underline{\dot{g}}_e}{J} \leq \vec{C}_{J-1}^{g_{e,t'}^s} \leq \frac{\overline{\dot{g}}_e}{J} \qquad (90)$$

11) Continuity constraints,

$$\left\{ C_{0,J}^{G_{g,t'}^s} = C_{J,J}^{G_{g,t'-1}^s}, C_{0,J}^{d_{e,t'}^s} = C_{J,J}^{d_{e,t'-1}^s}, C_{0,J}^{g_{e,t'}^s} = C_{J,J}^{g_{e,t'-1}^s} \right\} \quad (91)$$

$$C_{0,J}^{G_{g,t'}^s} \leq C_{J,J}^{G_{g,t'-1}^s} + M \cdot y_{g,t'} \qquad (92)$$

$$C_{0,J}^{G_{g,t'}^s} \geq C_{J,J}^{G_{g,t'-1}^s} - M \cdot z_{g,t'} \qquad (93)$$

$$C_{1,J}^{G_{g,t'}^s} - C_{0,J}^{G_{g,t'}^s} \leq C_{J,J}^{G_{g,t'-1}^s} - C_{J-1,J}^{G_{g,t'-1}^s} + M \cdot y_{g,t'} \qquad (94)$$

$$C_{1,J}^{G_{g,t'}^s} - C_{0,J}^{G_{g,t'}^s} \geq C_{J,J}^{G_{g,t'-1}^s} - C_{J-1,J}^{G_{g,t'-1}^s} - M \cdot z_{g,t'} \qquad (95)$$

The objective function (58) has two terms the first term represents the continuous-time expected operation cost (EOC) and second term shows the probability of sub-hourly WPC. Similarly, the weighting parameter $\beta \in [0, \infty)$ in the objective function (58) is to control the compromise between total cost and risk averse. In fact, if $\beta = 0$, the risk term in the objective function is ignored and the resulting problem becomes the risk neutral one. Additionally, by increasing the β value, the importance of the risk term is increased while it will be decreased for the total cost term. Constraint (59) refers to the happening of sub-hourly WPC in the unfavorable scenarios. In (59), variable $\vec{C}_{v,l}^{\Delta W_w^s(t)}$ shows the vectors of Bernstein coefficients related to sub-hourly WPC. Really, if a sub-hourly WPC occurs in scenario s or WPC for a sub-hourly

is larger than zero then the binary variable Ψ^s for scenario s becomes equal to 1, else it is 0 otherwise. Also, in (59) M is a large enough constant. Constraint (60) shows the total probability of sub-hourly WPCs in total set discrete scenarios. Also, total probability of sub-hourly WPCs must not be larger than λ value which is imposed by constraint (60). Additionally, in constraint (60), λ represents risk aversion or the maximum available risk of the decision maker. Equality constraint (61) is continuous-time form of objective function (1). Constraints (62)-(74), respectively, are similar to first-stage constraints (2)-(14), but these constraints are written in continuous-time formworks. Similarly, constraints (80)-(90) are similar to second-stage constraints (16)-(20), but these constraints are written in continuous-time formworks. Also, constraints (75)-(79) and constraints (91)-(95) are alike but for first and second stages continuity constraints, respectively. However, increasing order of Bernstein polynomial (i.e.,J) and number of scenario can increase accuracy proposed continuous-time risk model (or optimization problem) but it is likely to complicate the resultant model and makes it inefficient once the problem is implemented for a real-world systems. Accordingly, in other to reduce the complexity of the optimization problem, the following additional alternatives are also available:

• To implement a supercomputer,
• To implement the decomposition strategies [27],
• To utilize parallelization techniques [28],
• To apply appropriate techniques to simplify the power system and/or to reduce the number of scenarios and/or order of Bernstein polynomial, [29], [30] and [22],
• To decompose the transmission network by area [31].

V. CASE STUDIES

A. Modified IEEE Reliability Test System

To evaluate the performance of the proposed framework for the CT-RBUC model and discrete-time risk-based UC (DT-RBUC) model, some simulations have been executed on a single-area 24-bus IEEE Reliability Test System (RTS) [32]. Note that some of the characteristics of the RTS system have been modified to facilitate the simulation results. As can be seen in Fig.1, the RTS has 26 GUs, 2 wind farms (WFs), 2 ESUs, 17 demands and 38 lines. The data of GUs, demands and transmission lines are given in [32]. Daily peak load is 2873.75 MW and it happens at hour 21. Noted that, the GUs 24-29 have been replaced by WF-2 (as shown in Fig.1). Two WFs located at nodes 11 and 22, have installed capacities of 480 MW and 570 MW, respectively. The cost of WPC is assumed to be 20 \$/MWh. Two ESUs have been located at buses 14 and 17, as shown in Fig.1. The energy capacity, charging /discharging power rating, and ramping rate of the ESU are 500MWh, 100MW and 25MW/min, respectively, and the efficiency of charge/discharge is 90%. Two main storage technologies, viz., hydro pumped storage systems and aggregated battery energy storages, can be considered as ESU. Also, it is assumed the non-market based power system operation is going to be taken place, accordingly, the charging and discharging cost functions are assumed to be zero. The uncertainty for the wind power outputs is modeled through the 25 scenarios at the operation stage. The probabilities (π_s) of all the scenarios are identical and equal to 0.04. Note also that the scenario generation and reduction
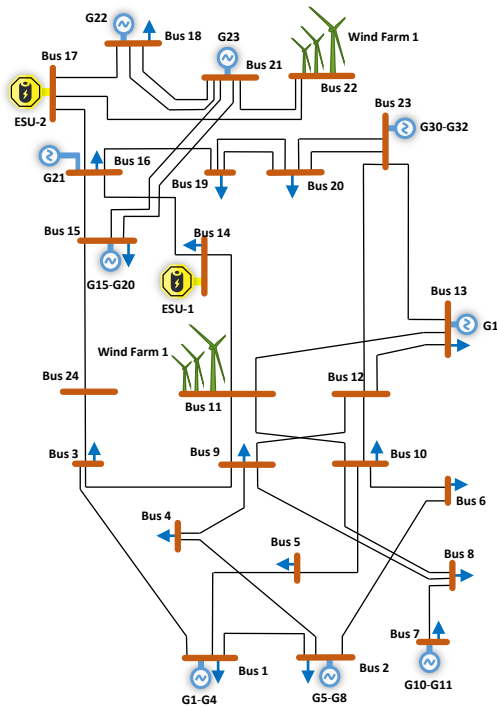
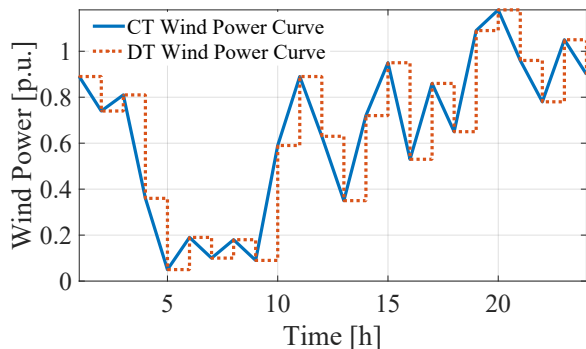Fig. 1: Modified IEEE reliability test system.

Fig. 2: The DT and CT wind power curves.

are outside the scope of this work. The BPs of degree 3 have been used to simulate the proposed CT-RBUC model. The wind power and demand profiles for the continuous-time (CT) and discrete-time (DT) are illustrated in Figs. 2 and 3, respectively. The following two case studies are analyzed:

Case 1: The discrete-time and continuous-time risk models without ESUs.

Case 2: The discrete-time and continuous-time risk model with ESUs.

The DT and CT risk models have been solved by CPLEX 12.6.2 on a PC with Intel Core-i7 processor at 4.2 GHz and 32 GB of RAM.

Case 1: The CT and DT risk models are solved by increasing the value of the risk parameter, β, by a step size of 1 from 0 to 7 to achieve the expected operation cost (EOC), number of committed units (NOCU), EWPC and λ, as shown in Figs. 4-7 and Table I. Fig. 4 shows the EOC, for two models as a function of β. It is inferred from this figure that the EOC, for two models, is not a linear function of β value. Also, increasing the β value can increase the EOC, for two models, because once β value is increased, the NOCU increases to provide the ramping requirements as seen in
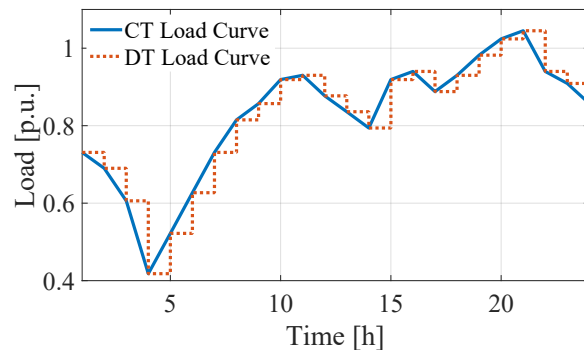
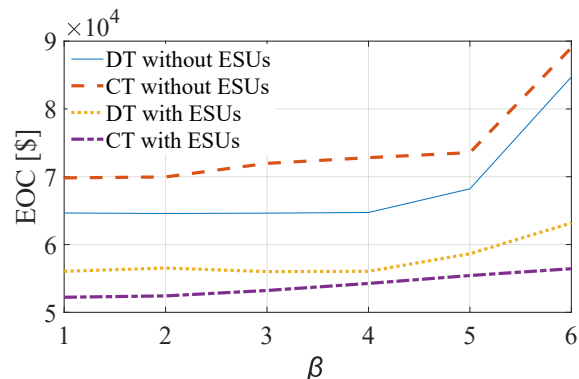

Fig. 3: The DT and CT load curves.

Fig. 4: The DT and CT load curves.

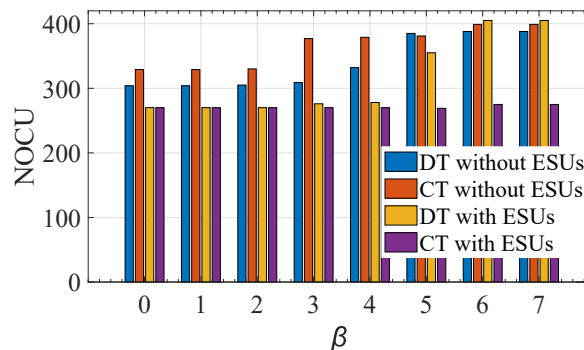Fig. 5: The NOCU for DT and CT risk models without/with ESUs under different β value.
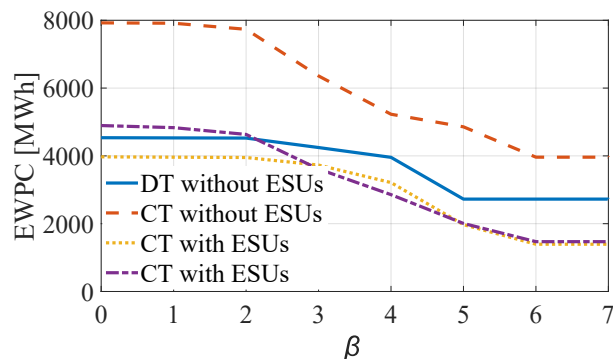

Fig. 6: The EWPC for DT and CT risk models without/with ESUs under different β value.

Fig.5. Also, the results for two models in Fig.4 indicate the minimum and maximum values of the EOC are obtained when β value is equal to 0 and 6, respectively. For instance, for the risk-neutral case, i.e.,
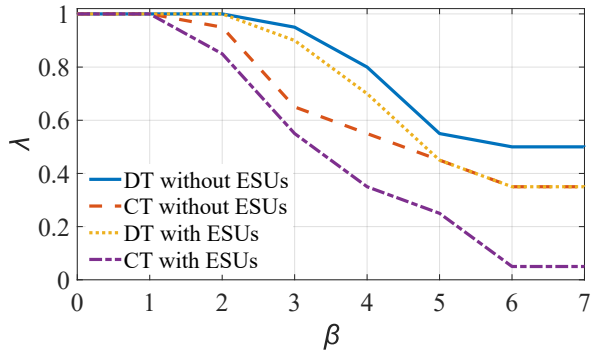
Fig. 7: The λ for DT and CT risk models without/with ESUs under different β value.
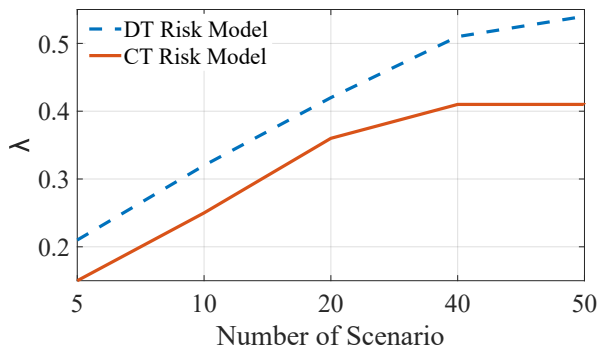

Fig. 8: DT and CT risk models under different scenarios; for $\beta = 4$.

$\beta = 0$, the EOCs for the CT and DT risk models are respectively 64653.33\$ and 69831.41\$. The increase in the EOC for the proposed CT risk model is expected because the proposed model commits more GUs to make a sub-hourly ramping requirement available (as shown in Fig.5) and curtails more WPG (as seen in Fig.6) to sustain the continuous-time load and generation balance. Also, as shown in Table I, for $\beta = 0$, the CT risk model commits expensive unit G2

TABLE I: The unit commitment results for DT and CT risk model with/without ESUs under $\beta = 0$ and 6.

Unit	DT risk model				CT risk model			
	Without-ESU		With-ESU		Without-ESU		With-ESU	
	$\beta=0$	$\beta=6$	$\beta=0$	$\beta=6$	$\beta=0$	$\beta=6$	$\beta=0$	$\beta=6$
1	0	1	0	1	0	1	1	1
2	0	1	0	1	1	1	1	1
3-4	1	1	1	1	1	1	1	1
5	0	1	0	1	0	1	0	1
6	0	1	0	1	0	1	1	1
7-9	1	1	1	1	1	1	1	1
10-11	1	1	1	1	1	1	0	1
12	0	0	0	1	0	1	0	1
13	0	0	0	0	0	1	0	1
14	0	1	0	0	0	0	0	0
15	0	0	0	1	0	0	0	0
16	0	1	0	1	0	0	0	0
17	0	1	0	1	0	0	0	0
18	0	1	0	1	0	0	0	0
19	0	1	0	1	0	0	0	0
20	1	0	1	1	1	0	1	0
21	1	0	1	0	1	0	1	0
22	1	1	1	1	1	1	1	1
23	1	1	1	1	1	1	0	1
30	1	1	1	1	1	1	1	1
31	1	1	1	1	1	0	1	0
32	1	1	1	1	1	1	1	0
Total	14	21	14	23	15	17	14	16

with high ramping capability at hour 21 (the peak load condition) to meet the extra ramping conditions taken by the CT-load model while it is disregarded in the DT risk model, wherein the unit G2 is off. As a result of committing this expensive GU, the EOC for the CT risk model is more increased than other models. Besides, for $\beta = 6$, the EOC increases significantly for two models, it is reasonable because in the case of larger values for β, in order to compensate variations of WPGs, the number of committed units, with high ramping capability, are increased to the highest value (as shown in Fig.5). For instance, as seen in Table I, for DT and CT risk models, the expensive units G16-G19 and G12-G13 are committed at peak hour 21, respectively. Also, this table shows that the commitment of the units is largely dependent on their ramping capability, especially to track the continuous-time WPG and load changes in CT risk model. This fact has been inferred from the results of Table I. Moreover, as can be seen in Table I, for $\beta = 6$, in the proposed CT risk model, the GUs G16-G19 are not committed in the hour 21, instead the GUs G12-G13 with more than 4 times ramping capacity have been turned on to be responsible for the fast changes caused simultaneously by WPGs and loads for the duration of hours 20–22. The results certify that the continuous-time ramping of GUs in the CT risk model would adjust the day-ahead scheduling of GUs such that the combination of the online GUs is better to react to the sub-hourly changes of the WPG and load in real-time operation. Accordingly, in the daily operation, it is practically essential to guarantee that the continuous-time ramping routes of GUs can supply the ramping conditions of WPG and load profiles, when the β value increases, in real-time operation. Fig. 6 shows the expected WPC (EWPC) under different β values, from this figure the following considerations are observed: (i) The EWPC decreases by increasing the value of β; The decrement in the EWPC is due to the fact that by increasing β, the system operator (SO) wants to become more risk averse, therefore, the SO commits more GUs to purchase more reserve deployments for some undesired scenarios. On the other hand, for the higher values of β, i.e., $\beta > 4$, the problem commits an additional GU to provide an extra scheduled reserve while it would be more cost-effective than WPC. (ii) It is observed that the EWPC in the CT risk model is less reduced than another model under different values of β; the reason is that to compensate the continuous-time variations of WPG, it is needed to commit additional fast-ramping GUs that these GUs are usually expensive, so, the WPC option would be more cost-effective than committing additional expensive GUs. Alternatively, in the CT risk model, the most ramping capacity of the online GUs are used to supply the ramping requirement of the load variations not wind variations. Also, in the case of $\beta = 0$, the WPC probability (λ) for two models is equal to 100%, which means the WPC happens in all scenarios. Also, Fig. 7 depicts more numerical details about λ for different values of β. As can be seen in this figure, the λ value is reduced in both models. However, by increasing the β value, the λ value in the proposed CT risk model is more reduced than other models. This is basically due to the fact that in the proposed CT risk model, the SO can allocate more sub-hourly reserve from the online GUs to have less forced WPC encountering with undesired scenarios. From Fig. 7, this fact can be clearly understood that the proposed CT risk model outperforms compared to the DT risk model in terms of risk aversion or λ reduction.

Case 2: The DT and CT risk models with the two ESUs have

been studied here (location of ESUs has been shown in Fig. 1). The EOC, NOCU, EWPC and λ values associated with the DT and CT risk models with ESUs support, for comparing with Case 1, are provided in Figs. 4-7 and Table I. In the previous case, the scarcity of ramping capacity is the main obstacle to decrease the EOC, EWPC and λ values. Accordingly, in this case, if there was no ESU in the joint scheduling system, the system would partially overcome this scarcity by committing new GUs. Also, if there was the ESU in the joint scheduling system, the system could overcome this scarcity by high ramping capability of ESU's charging/discharging power. In Fig. 4, the ESU inclusion in both models reduces the EOC for different β values, but the CT risk model yields a higher cost saving than the DT risk model. This was expected, because comparing the obtained results in Fig. 5 and 6 with and without ESUs support, for both models, shows that the NOCU and EWPC are decreased by ESUs support. Besides, Fig. 4 shows that with ESU support, the EOC for CT risk model, under different β values, is more decreased than the other model. The reason is that in the CT risk model when β increases from 0 to 6, the NOCU increases fewer than DT risk owing to the ability of CT risk to better manage ramping capacity of ESUs, this fact is revealed in Fig. 5. Furthermore, the ESU inclusion in CT risk model will more moderate the GUs cycling in the hours 19-22 (peak time), and will eliminate the need for committing expensive GUs during these hours. For example, as shown in Table I, for the constant β (i.e. $\beta = 6$), in the CT risk model without ESUs an additional GU, i.e., G32, is committed at the peak hour 21, but this is not the case in this model with ESUs while G32 is not committed. Fig. 6 shows the EWPC for both models under different β values in cases with ESUs. This figure shows that ESUs inclusion in both models has a positive effect on the EWPC reduction. But, this reduction in the CT risk model is more than DT risk model because the ESUs utilization in CT risk model better revises the scheduling of GUs with respect to the DT risk model, while the CT risk model efficiently schedules the daily operation of both ESUs and GUs which causes to increase the utilization of WPGs and decrease the EWPC value. On the other hand, the DT risk model does not generate ramping route of ESUs, however the ESUs in the proposed CT risk framework directly optimizes the continuous-time ramping route. Also, the λ value as a function of the β value for both models with ESU is given in Fig. 7. Interesting insights can be inferred from the figure as: (i) the values of λ for both models with ESUs are decreased as the value of β increases. Also, this figure indicates that the λ value for CT risk model is more reduced than the other model, which is vice versa in the previous case. The reason is that, with ESUs application in the CT risk model, the additional reserve would be more economical than the WPC in some scenarios, as seen in Fig. 7, thus, the value of λ in both models are more decreased in the higher values of β than these models without ESUs. Also, the ESUs in the CT risk model, would more improve the implementation of ramping capacity of GUs in some undesired scenarios than other models. (ii) This figure shows that the risk aversion of the CT risk model is largely dependent on the β value, especially in the case with ESU support. In this condition, the SO can choose a proper value of β to increase the allocated reserves from the ESUs and GUs to have less forced WPC encountering with the undesired scenarios. Accordingly, by increasing β, the percentage of λ over the entire scheduling horizon is decreased due to more reserves allocated by the resources.

TABLE II: The EWPC and EOC for DT and CT models under different number of ESUs; for $\beta = 4$.

Number of ESUs	EWPC [MWh]		EOC [M$]	
	DT-model	CT-model	DT-model	CT-model
0	5143.4	5421.5	2.16	2.21
3	3234.68	2954.68	1.97	1.91
6	1902.45	1532.34	1.85	1.73

TABLE III: Comparing our proposed CT risk model with other risk models in [26]; for $\beta = 4$.

	EWPC[MWh]	EOC [M$]	Time [min]
Proposed CT risk model	2854.68	1.90	35
Risk model in [26]	4234.68	2.3	23

B. Modified IEEE 118-bus System

In this section, the modified IEEE-118 bus system is used as a large-scale power system with 54 thermal generators, 3 wind farms, 186 transmission lines and 91 load buses. Parameters of load profiles, thermal units and transmission network are given at motor.ece.iit.edu/data/SCUC_118. In other to model the system congestion the line flow limits for a few transmission lines are reduced to 100 MW. Three wind farms at buses 32, 49 and 77 are installed. Three wind farm generation profiles follow the same pattern as that of the previous test system which are scaled by factor of 4. The generation capacity of these wind farms is 1200 MW. The peak load at this system is 3733 MW. Therefore, the penetration level of the available WPG is 32.14% in this system. The cost of WPC is assumed to be 25 $/MWh. Three ESUs are at buses 32, 49 and 77 which have the same capacity and parameters of the previous test system. The uncertainty for the wind power outputs is modeled through 10 discrete scenarios at the operation stage. The probabilities (π_s) of all the scenarios are identical and equal to 0.1. Note also that the scenario generation and reduction are outside the scope of this work. The BPs of degree 3 (or $J = 3$) have been used to simulate the proposed CT risk model. The wind power and demand profiles follow the same pattern as that of the previous test system.

In this section, four cases are studied:

Case 1: Effect of order of Bernstein polynomial on proposed risk model results.

Case 2: The sensitivity analysis for probability of wind power curtailment under different scenarios.

Case 3: Impact of increasing the number of ESUs on the EWPC and EOC.

Case 4: Comparing our proposed risk model with other models.

For each case, the proposed risk model solution results by DT and CT risk models are compared.

Case 1: In this case effect of order of Bernstein polynomial or J value in CT model on solution results has been studied. Table II compares the results obtained from different J. It is apparent from this table that the EWPC, EOC and λ values are decreased by increasing J value but at this time the solution time is increased. This result is expected. However, the reason for this is that there is a positive correlation between J and ability of CT model. In fact, the performance of CT model to manage ramping capacity of ESUs is increased by rising J value. As can be seen in Table II, as expected a positive correlation is find between J value and solution time. A possible explanation for increasing solution time may be

that continuous variables in CT model is increased with increasing J value, and also, the size of problem increased. Therefore, it is predictable that the computation time and memory consumption is higher for CT formulation. By the way, as this is an offline practice which is performed in the prior day, execution time is not of utmost importance.

Case 2: This case studied the effect of different number of scenarios on DT and CT risk models results. According to Fig. 8, the number of generated scenarios for both DT and CT risk models have been assigned. As can be seen in Fig. 8, it is clear that the λ value for both DT and CT risk models rose considerably between 5 and 40 (number of scenarios). Furthermore, the trends for both commodities were very similar, and so a positive correlation between number of scenarios and the λ value is suggested. What is interesting about the data in Fig.8 is that, over the following 20 scenarios the λ values for CT model remained relatively stable, but, for the DT model over the following 40 scenarios the trends of the λ value is slightly decreased. This result implies that the proposed CT risk model needs a lower number of scenarios than the DT risk model to determine the optimal the λ values.

Case 3:In this case impact of different number of ESUs on the EWPC and EOC results has been studied. It can be seen from the data in Table III that the EWPC and EOC value for both DT and CT risk models are decreased. But, for similar number of ESUs, the EWPC nad EOC values in CT risk model are more reduced than DT risk model. These results are expected, because the fast ramping capacity has been more increased than DT model with increase number of ESUs in power system, additionally, the CT model has more capability in handling fast ramping capacity than the DT model.

Case 4: Here the EWPC, EOC and solution time results for the proposed CT risk model with other similar risk model, i.e., [26], with ESUs are compared. We assume that β value is 4. The results obtained from this comparison are given in Table IV. What is interesting about the data in this table is that our proposed CT risk model outperforms the other risk model (in [26]) in terms of EWPC and EOC reduction. This result is expected. The reason for this is probably that the risk model in [26] modeled by a DT model, so, this risk model cannot handle fast ramping capability of ESUs to follow fast sub-hourly variation of WPG over scheduling horizon. But, as Table IV shows, there is a significant difference solution times between the two risk models. In fact, there are several reasons for this difference. A possible explanation for this significant difference may be that our proposed risk model has more variables and equality/inequality constraints.

VI. CONCLUSIONS

This paper presents a two-stage stochastic risk model to minimize probability of occurring sub-hourly WPC using discrete-time and continuous-time frameworks with ESUs. The proposed stochastic risk model characterizes the uncertain nature of WPG. The uncertainty of WPG is modeled through a number of probable scenarios. This paper proposes a novel model for ESUs operation based on continuous-time framework. The proposed continuous-time model ensures the optimality of the ESUs operation by maintaining the continuity of the decision routes, and uniquely schedules for continuous-time ramping, power, and energy routes of the ESUs and captures their ultimate flexibility to compensate

the continuous-time variation of WPGs. All researchers that have utilized risk-based stochastic optimization approach to measure probability of WPC or load shedding in power systems, use conventional discrete-time framework to model the trade-off between minimizing the EOC and the probability of WPC in the undesired scenarios. Accordingly, in this paper a novel risk assessment based on continuous-time framework has been presented to minimize the probability of occurring sub-hourly WPC. Also, the impacts of different values of risk aversion parameter on the optimal solution of the DT and CT risk problems have been investigated in two cases, namely with and without ESU support. Considering the theoretical properties of the proposed model and the results of the case studies conducted on the IEEE-RTS and modified IEEE-118 bus system the conclusions below are in order:
• According to the results, it is observed that the EOC, NOCU, EWPC and WPC probability in the proposed continuous-time optimization model reduce more than the discrete-time model.
• The results show that the EWPC and WPC probability (λ) in CT model with ESUs reduces more than the DT model with ESUs. These results confirm the superiority of the CT model compared to the DT model to make better use of the fast ramping capability of the ESUs.
• What is interesting about the results in this paper is that the CT model reduces the cycling of the expensive GUs by ignoring expensive GUs in peak hours; for this reason, the EOC, NOCU in CT model reduce more than the DT model.
• The correlation between β and the role of ESUs in CT model is interesting because by increasing β, the role of ESUs in power system operation can be changed.
• The simulation results of the modified IEEE-118 bus system show that the proposed CT risk model can be applied by the large-scale power systems with acceptable solution time.

REFERENCES

[1] Ahmad Nikoobakht, Jamshid Aghaei, Miadreza Shafie-khah, and J. P. S. Catalão, "Assessing Increased Flexibility of Energy Storage and Demand Response to Accommodate a High Penetration of Renewable Energy Sources," Transactions on Sustainable Energy, 2018.
[2] R. T. Elliott, R. H. Byrne, J. C. Neely, C. A. Silva Monroy, D. A. Schoenwald, and L. Grant, "Impact of Increased Renewable Energy Penetration on Small Signal Stability in the WECC," Sandia National Laboratories2012.
[3] C. A. S. Monroy and R. D. Christie, "Energy storage effects on day-ahead operation of power systems with high wind penetration," in 2011 North American Power Symposium, 2011, pp. 1-7: IEEE.
[4] Y. Dvorkin, R. Fernandez-Blanco, D. S. Kirschen, H. Pandžić, J.-P. Watson, and C. A. J. I. T. o. P. S. Silva-Monroy, "Ensuring profitability of energy storage," vol. 32, no. 1, pp. 611-623, 2016.
[5] X. Dui, G. Zhu, and L. Yao, "Two-stage optimization of battery energy storage capacity to decrease wind power curtailment in grid-connected wind farms," IEEE Transactions on Power Systems, vol. 33, no. 3, pp. 3296-3305, 2018.
[6] J. Aghaei, A. Nikoobakht, M. Mardaneh, M. Shafie-khah, and J. P. Catalão, "Transmission switching, demand response and energy storage systems in an innovative integrated scheme for managing the uncertainty of wind power generation," International Journal of Electrical Power & Energy Systems, vol. 98, pp. 72-84, 2018.
[7] C. O'Dwyer, L. Ryan, and D. Flynn, "Efficient large-scale energy storage dispatch: challenges in future high renewable systems," IEEE Transactions on Power Systems, vol. 32, no. 5, pp. 3439-3450, 2017.
[8] Y. Wen, C. Guo, H. Pandžić, and D. S. Kirschen, "Enhanced security-constrained unit commitment with emerging utility-scale energy storage," IEEE Transactions on power Systems, vol. 31, no. 1, pp. 652-662, 2015.
[9] M. Parvania, M. Fotuhi-Firuzabad, and M. Shahidehpour, "Comparative hourly scheduling of centralized and distributed storage in day-ahead markets," IEEE Transactions on Sustainable Energy, vol. 5, no. 3, pp. 729-737, 2014.

[10] A. Nikoobakht, J. Aghaei, T. Niknam, H. Farahmand, and M. Korpås, "Electric vehicle mobility and optimal grid reconfiguration as flexibility tools in wind integrated power systems," International Journal of Electrical Power & Energy Systems, vol. 110, pp. 83-94, 2019.

[11] T. Li, M. Shahidehpour, and Z. Li, "Risk-constrained bidding strategy with stochastic unit commitment," IEEE Transactions on Power Systems, vol. 22, no. 1, pp. 449-458, 2007.

[12] S. Abedi, M. He, and D. Obadina, "Congestion risk-aware unit commitment with significant wind power generation," IEEE Transactions on Power Systems, vol. 33, no. 6, pp. 6861-6869, 2018.

[13] R. Billinton, B. Karki, R. Karki, and G. Ramakrishna, "Unit commitment risk analysis of wind integrated power systems," IEEE Transactions on Power Systems, vol. 24, no. 2, pp. 930-939, 2009.

[14] K. Hreinsson, B. Analui, and A. Scaglione, "Continuous Time Multi-stage Stochastic Reserve and Unit Commitment," in 2018 Power Systems Computation Conference (PSCC), 2018, pp. 1-7: IEEE.

[15] M. Parvania and R. Khatami, "Continuous-time marginal pricing of electricity," IEEE Transactions on Power Systems, vol. 32, no. 3, pp. 1960-1969, 2016.

[16] M. Parvania and A. Scaglione, "Unit commitment with continuous-time generation and ramping trajectory models," IEEE Transactions on Power Systems, vol. 31, no. 4, pp. 3169-3178, 2015.

[17] L. Baringo and A. J. Conejo, "Offering strategy of wind-power producer: A multi-stage risk-constrained approach," IEEE Transactions on Power Systems, vol. 31, no. 2, pp. 1420-1429, 2015.

[18] T. Li and M. Shahidehpour, "Strategic bidding of transmission-constrained GENCOs with incomplete information," IEEE Transactions on power Systems, vol. 20, no. 1, pp. 437-447, 2005.

[19] T. Li and M. Shahidehpour, "Risk-constrained FTR bidding strategy in transmission markets," IEEE Transactions on Power Systems, vol. 20, no. 2, pp. 1014-1021, 2005.

[20] A. Nikoobakht, J. Aghaei, M. Parvania, and M. Sahraei-Ardakani, "Contribution of FACTS devices in power systems security using MILP-based OPF," IET Generation, Transmission & Distribution, 2018.

[21] A. Castillo, C. Laird, C. A. Silva-Monroy, J.-P. Watson, and R. P. O'Neill, "The unit commitment problem with AC optimal power flow constraints," IEEE Transactions on Power Systems, vol. 31, no. 6, pp. 4853-4866, 2016.

[22] X. Chen, J. Tan, Z. Liu, and J. Xie, "Approximation of functions by a new family of generalized Bernstein operators," Journal of Mathematical Analysis and Applications, vol. 450, no. 1, pp. 244-261, 2017.

[23] M. Izadi and A. Safdarian, "A MIP model for risk constrained switch placement in distribution networks," IEEE Transactions on Smart Grid, vol. 10, no. 4, pp. 4543-4553, 2018.

[24] J. Zhao, C. Wan, Z. Xu, and J. Wang, "Risk-based day-ahead scheduling of electric vehicle aggregator using information gap decision theory," IEEE Transactions on Smart Grid, vol. 8, no. 4, pp. 1609-1618, 2015.

[25] M. Asensio and J. Contreras, "Risk-constrained optimal bidding strategy for pairing of wind and demand response resources," IEEE Transactions on Smart Grid, vol. 8, no. 1, pp. 200-208, 2015.

[26] X. Cao, J. Wang, J. Wang, and B. Zeng, "A Risk-Averse Conic Model for Networked Microgrids Planning With Reconfiguration and Reorganizations," IEEE Transactions on Smart Grid, vol. 11, no. 1, pp. 696-709, 2019.

[27] R. Rahmaniani, T. G. Crainic, M. Gendreau, and W. Rei, "The Benders decomposition algorithm: A literature review," European Journal of Operational Research, vol. 259, no. 3, pp. 801-817, 2017.

[28] A. Papavasiliou and S. S. Oren, "Multiarea stochastic unit commitment for high wind penetration in a transmission constrained network," Operations Research, vol. 61, no. 3, pp. 578-592, 2013.

[29] X. Cheng and T. J. Overbye, "PTDF-based power system equivalents," IEEE Transactions on Power Systems, vol. 20, no. 4, pp. 1868-1876, 2005.

[30] J. M. Morales, S. Pineda, A. J. Conejo, and M. Carrion, "Scenario reduction for futures market trading in electricity markets," IEEE Transactions on Power Systems, vol. 24, no. 2, pp. 878-888, 2009.

[31] A. Ahmadi-Khatir, A. J. Conejo, and R. Cherkaoui, "Multi-area unit scheduling and reserve allocation under wind power uncertainty," IEEE Transactions on power systems, vol. 29, no. 4, pp. 1701-1710, 2013.

[32] R. T. Force, "The IEEE reliability test system-1996," IEEE Trans. Power Syst, vol. 14, no. 3, pp. 1010-1020, 1999.